Discovery of a novel DYRK1A Inhibitor with neuroprotective activity by virtual screening and *in vitro* biological evaluation

Xinxin Si
School of Pharmacy, Jiangsu Ocean University

Chenliang Qian
School of Pharmacy, Jiangsu Ocean University https://orcid.org/0009-0009-6837-5320

Nianzhuang Qiu
School of Pharmaceutical Sciences, Shandong First Medical University & Shandong Academy of Medical Sciences https://orcid.org/0009-0007-6786-1269

Yaling Wang
School of Pharmacy, Jiangsu Ocean University

Mingli Yao
School of Pharmacy, Jiangsu Ocean University

Hao Wang
School of Pharmaceutical Sciences, Shandong First Medical University & Shandong Academy of Medical Sciences https://orcid.org/0000-0002-6972-8900

Xuehui Zhang
School of Pharmaceutical Sciences, Shandong First Medical University & Shandong Academy of Medical Sciences https://orcid.org/0009-0009-1014-8918

Jie Xia (jie.william.xia@hotmail.com)
State Key Laboratory of Bioactive Substance and Function of Natural Medicines, Institute of Materia Medica, Chinese Academy of Medical Sciences and Peking Union Medical College
https://orcid.org/0000-0002-9567-3763

Research Article

Keywords: DYRK1A, virtual screening, pharmacophore model, molecular docking, molecular dynamics simulation

Posted Date: November 3rd, 2023

DOI: https://doi.org/10.21203/rs.3.rs-3544939/v1

Abstract

Dual specificity tyrosine phosphorylation regulated kinase 1A (DYRK1A) is implicated in accumulation of amyloid β-protein (Aβ), phosphorylation of Tau proteins, and may eventually cause neurodegenerative diseases. Though many DYRK1A inhibitors have been discovered, there is still no marketed drug targeting DYRK1A. This is partly due to the lack of effective and safe chemotypes; therefore, it is still necessary to identify new classes of DYRK1A inhibitors. By the design of a virtual screening workflow composed of pharmacophore modeling and molecular docking and the following practical application, we identified compound **L9**, ((Z)-1-(((5-phenyl-1H-pyrazol-4-yl) methylene)-amino)-1H-tetrazol-5-amine), as a moderately active DYRK1A inhibitor (IC_{50}: 1.67 μM). This compound was structurally diverse compared with the known DYRK1A inhibitors, showed a unique binding mode to DYRK1A, and was not toxic to either SH-SY5Y cells or HL-7702 hepatocytes (IC_{50} 100 μM). Furthermore, compound **L9** showed neuroprotective activity by regulating the expression of Aβ and phosphorylation of Tau protein. In conclusion, we have identified a novel DYRK1A inhibitor through virtual screening and *in vitro* biological evaluation, which holds the promise for further study.

1. Introduction

Dual-specificity tyrosine-regulated kinases (DYRKs) belong to the CMGC kinase group, which include five isoforms in mammals [1], i.e., DYRK1A, DYRK1B, DYRK2, DYRK3, and DYRK4. Among these, DYRK1A is most extensively studied. This protein is encoded by the gene of *dyrk1a* on the Down syndrome (DS) critical region chromosome 21 (DSCR) [2] and comprises 763 amino acids. It includes a nuclear localization signal at the N-terminus, a kinase domain, a PEST (proline, glutamate, serine and threonine) domain for protein degradation, a 13-consecutive-histidine repeat, and a S/T-rich region that has an unknown function [3, 4].

DYRK1A interacts with diverse substrates [5]. As a dual-substrate-specific protein kinase, it could phosphorylate tyrosine residue Tyr321 of its own activation loop as well as to phosphorylate other substrates at serine or threonine residues [6]. Extensive studies have demonstrated the indispensable role of DYRK1A in numerous critical biological processes. For instance, DYRK1A participates in the selective splicing of pre-mRNAs implicated in embryonic neurogenesis [7]. Additionally, DYRK1A modulates angiogenesis through activating the nuclear factor of activated T-cells (NFATc) signaling pathway [8]. Due to its location in DSCR, overexpression of DYRK1A may result in cerebellar malformations, reduction in cortical neurons, and synaptic abnormality [9]. Overactivation of DYRK1A is linked to a range of diseases, such as neurodegenerative disorders [10, 11], diabetes mellitus [12, 13], and cancers [14–16]. Accordingly, DYRK1A Inhibition may reverse the aforementioned diseases and thus DYRK1A is regarded as a potential drug target.

To date, many DYRK1A inhibitors have been identified (cf. Figure 1), but no compound has been approved for clinical use. Epigallocatechin gallate (EGCG) (**1**), a polyphenol highly contained in green tea [17], is currently undergoing Phase II clinical trials for Alzheimer's disease (AD) [18]. Harmine (**2**), a β-

carboline alkaloid with the IC_{50} value of 33 nM for DYRK1A, inhibits neuritogenesis [19]. However, it may cause the side effect of hallucination. Leucettamine L_{41} (**3**), a compound obtained from porous animal sponges (IC_{50}:28 nM for DYRK1A) [20], is also effective to attenuate memory impairment and cognitive deficits in mice [21]. Apart from natural products, synthetic compounds could also show DYRK1A inhibition. INDY (**4**) is a potent DYRK1A inhibitor (IC_{50}: 240 nM) [22]. Another DYRK1A inhibitor, Lorecivivint (**5**) could block Wnt/β-catenin pathway and is currently in phase III clinical trial for osteoarthritis [23, 24]. The exact structure of SM07883 (**6**) is undisclosed, but it is currently in phase I clinical trial for AD due to its high potency for DYRK1A, good membrane permeability and high oral bioavailability [25].

Virtual screening (VS) could fast identify novel hit compounds in a cost-effective way, when coupled with *in vitro* bioassays. Several research groups have identified DYRK1A inhibitors from chemical library using such a strategy. Gourdain *et al.* used molecular docking-based VS to identify DYRK1A inhibitor. After structural optimization, they identified one highly active compound DANDY (**7**), with the IC_{50} value of 3 nM [26]. It is likely that the excessive hydroxyl groups affect its blood-brain barrier permeability and thus is not under active development. Koyamaet *et al.* constructed a logistic regression model based on residue binding free energy and a pharmacophore model to screen a focused library [27] and identified two DYRK1A inhibitors (**8, 9**) that are active at the micromolar concentrations [28].

To the best of our knowledge, the outcome of the known classes of DYRK1A inhibitors in clinical trials and preclinical development is unpredictable, and thus novel chemotypes are still needed as the backup series of DYRK1A inhibitors. According to the above cases of success, VS could facilitate the achievement of this specific aim. In this study, we aim to identify structurally diverse DYRK1A inhibitors for neurodegenerative diseases by VS. A computational workflow was rationally designed, which was composed of pharmacophore modeling and molecular docking. With that workflow, we screened our in-house chemical library, identified 10 potential hits and tested them for DYRK1A inhibition. As a result, we discovered a new DYRK1A inhibitor **L9**, with (Z)-1-(1H-pyrazol-4-yl)-N-(1H-tetrazol-1-yl) methanimine as its core scaffold. We performed molecular dynamics simulations to gain insights into the details of its binding to DYRK1A and provide clues for further optimization. Next, we assessed the protective effect of compound **L9** on OA-induced neuronal cells, and its cytotoxicity to SH-SY5Y cells and HL-7702 hepatocytes. Lastly, we preliminarily explored molecular mechanism of compound **L9** by western blot assay.

2. Results and Discussions

2.1. Virtual Screening

2.1.1. Pharmacophore Model

We selected six DYRK1A inhibitors from the article of Gourdain *et al.* [29] to comprise a training set (cf. Figure 2a, A1-A6). Next, we utilized the Catalyst/HipHop module of Discovery Studio (v16.1.0, Dassault Systèmes Biovia Corp) to generate 10 common-feature pharmacophore models (cf. Figure 2b). The data for these models are presented in Table 1. The rank of 10 models ranged from 41.578 **(Pharm_01)** to 36.842 (**Pharm_10**). The values of Direct Hit, Partial Hit and Max Hit were the same for 10 models. To be specific, Direct Hit equal to 111111 and Partial Hit as 000000 indicated six DYRK1A inhibitors fully matched the pharmacophore. Max Hit was 3, meaning that the input ligand could match up to 3 features.

Table 1
The parameters of 10 common-feature pharmacophore models generated with the Catalyst/HipHop module of Discovery Studio.

Model	Features [a]	Rank	Direct Hit [b]	Partial Hit [c]	Max Fit[d]
Pharm_01	RAA	41.578	111111	000000	3
Pharm_02	RAA	40.700	111111	000000	3
Pharm_03	RAA	40.215	111111	000000	3
Pharm_04	RHA	39.562	111111	000000	3
Pharm_05	RHA	39.296	111111	000000	3
Pharm_06	RHA	37.544	111111	000000	3
Pharm_07	RRH	36.905	111111	000000	3
Pharm_08	RRH	36.905	111111	000000	3
Pharm_09	RRH	36.842	111111	000000	3
Pharm_10	RRH	36.842	111111	000000	3

[a] H, general hydrophobic feature; A, hydrogen bond acceptor; R, ring aromatic.

[b] Direct Hit: 1, a ligand fully matches the pharmacophore; 111111, all the ligands fully match the pharmacophore;

[c] Partial Hit: 1, a ligand partially rather than fully matches the pharmacophore; 000000, no ligand partially matches the pharmacophore.

[d] Max Fit: The maximal features that the input compound can match.

In order to select the optimal model, we collected 20 additional compounds from the same article (cf. Figure 3a, A7-A22) to comprise a test set and assessed model performance in discriminating between highly active compounds (IC_{50} < 100 nM) and weakly active ones ($IC_{50} \geq$ 100 nM). According to Fig. 3b, **Pharm_04** was the optimal model that could best assign high fitvalue scores to the highly active compounds and low fitvalue scores to the weakly active compounds. Figure 3c illustrates that **Pharm_04** was composed of three pharmacophore features, i.e., one ring aromatic (orange), one general hydrophobic feature (blue) and one hydrogen bond acceptor (green).

2.1.2 Virtual screening

The workflow of virtual screening is described in Scheme 1, including pharmacophore filtering with the aforementioned model **Pharm_04**, molecular docking with Smina, visual inspection of binding modes, and molecular clustering based on FCFP_6 fingerprints.

The in-house chemical library (i.e., the compounds originally purchased from ChemDiv and Specs, 16,828 compounds) was used for screening. As the pharmacophore model **Pharm_04** comprised three features, the fitness score for a perfect match to the pharmacophore was 3. Accordingly, we used the pharmacophore fitness value of 1.5 (50% match) as the cutoff. Consequently, we retained a total of 1,381 molecules. The crystal structure of human DYRK1A protein (PDB code: 6S14) was utilized for molecular docking by smina (https://github.com/mwojcikowski/smina) [30], as it is in high resolution and in complex with a potent inhibitor. We selected top-scoring 200 compounds based on their Minimized Affinity scores (-11.85 ~ -8.10 kJ/mol). According to the ligand-protein interactions observed from the cocrystal structure and the findings of Ogawa *et al*. [22], the hydrogen bonds with Lys188 and Leu241 play a crucial role in ligand-protein recognition. The visual inspection of the binding modes led to the identification of 57 compounds that formed hydrogen bonds with Lys188 or Leu241. Finally, the compounds were clustered into 10 clusters based on FCFP_6 fingerprints. We selected one chemical structure from each cluster, with priority given to the compounds exhibiting high FitValue scores, low Minimized Affinity scores, and better synthetic feasibility. By searching PubChem (https://pubchem.ncbi.nlm.nih.gov/) and SciFinder (https://scifinder-n.cas.org/), we confirmed that DYRK1A inhibitory activity of these compounds had not been reported before (cf. Table 2).

2.1.3. Experimentally validated hits

We evaluated the inhibitory activity of 10 potential compounds against DYRK1A at the concentration of 10 μM. As shown in Table 2, compound **L9** was experimentally validated as a DYRK1A inhibitor, with the IC_{50} value of 1.67 μM (cf. Figure 4a). By calculating structural similarity between compound **L9** and the known DYRK1A inhibitors ($IC_{50} \leq 10$ μM, 1,160 compounds) that we collected from ChEMBL33 (https://www.ebi.ac.uk/chembl/, accessed May. 2023), we confirmed that compound **L9** represented a novel chemotype of DYRK1A inhibitors because the maximum structural similarity (Tanimoto coefficient) based on FCFP_6 fingerprints was as low as 0.24 (cf. Figure 4b). The compound that had the maximum similarity to compound **L9** was CHEMBL2234269, with the IC_{50} value of 10 μM. In addition, we calculated the structural similarity based on FCFP_6 fingerprints between compound **L9** and the cognate ligand **KQW** from the cocrystal structure used for molecular docking (cf. Figure 4c). The result showed that the similarity between them was only 0.06, indicating the effectiveness of our computational workflow for scaffold hopping.

2.2. Plausible binding modes from molecular dynamics simulation

To further analyze the interactions between compound **L9** and the DYRK1A protein, we performed 100-ns molecular dynamics simulation using GROMACS (version 2019.4) [31]. The RMSDs of the heavy atoms of DYRK1A and compound **L9** over the simulation time are depicted in Fig. 5a. The protein-ligand binding mode was extracted from the trajectory after equilibration, which is presented in Fig. 5b. As shown in the figure, the pyrazole scaffold of the chemical structure formed hydrogen bonds with Glu239 and Leu241 (a conserved residue existing in protein binding with most DYRK1A inhibitors [22]). In addition, the tetrazole fragment interacted with Asn244 by hydrogen bonding. π-σ interactions existed between the benzene ring and Leu294/Val173, as well as between the tetrazole fragment and Ile165. Additionally, there was a plausible halogen bond between the pyrazole scaffold and Met240, and a π-alkyl interaction between the benzene ring and Val222/Lys199/Ala186.

To clearly show the capacity of our computational workflow in scaffold hopping, we analyzed the binding mode between compound **KWQ**, the ligand from the cocrystal structure, and DYRK1A (PDB ID: 6S14) (cf. Figure 5c). This figure shows that the binding mode between compound **KWQ** and DYRK1A was different from that between **L9** and DYRK1A. Though it also keeps the hydrogen bond with Leu241, the difference is that the dihydropyrazolo-pyridazine fragment establishes a hydrogen bond with Lys188, and the pyrimidine moiety interacts with Glu239 through a carbon-hydrogen bond. We found that the IC_{50} of compound **KQW** on DYRK1A is 0.11 μM [32], ten times more potent than our hit compound **L9** (IC_{50} = 1.69 μM). Based on the comparative study of the two binding modes, we proposed a hypothesis that the absence of hydrogen bond between **L9** and Lys188 may lead to the reduced DYRK1A inhibition. This provided us with a direction to modify the compound **L9**. For instance, the benzene ring in the structure of compound **L9** could be replaced by a fragment of hydrogen-bond acceptor, such as pyridine, to introduce a potential hydrogen bond with Lys188.

2.3. Neuroprotective activity

In order to predict whether compound **L9** had the potential for AD, we tested neuroprotective activity of compound **L9** for OA-induced SH-SY5Y cells. Figure 5a demonstrates a statistically significant reduction in the cell viability of SH-SY5Y cells that were exposed to OA (100 nM). The compound **L9** exhibited neuroprotection at the concentration of 10 μM (cf. Figure 6a). Notably, we observed that the positive drug Harmine attenuated OA-induced damage at the concentration of 1 μM but not at the concentration of 10 μM. As Fig. 6b showed that compound **L9** at 10 μM and Harmine at 1 μM had no effect on SH-SY5Y cells, we excluded the effect of compound **L9** or Harmine itself on cell viability, thus further confirmed the neuroprotective effect on SH-SY5Y cells.

2.4. Cytotoxicity Evaluation

In order to assess cytotoxicity of the compounds, we measured cell viability of SH-SY5Y cells and HL-7702 hepatocytes after the treatment of compound **L9** using CCK-8 assay. Figure 6c demonstrates that compound **L9** was not toxic to either SH-SY5Y cells or HL-7702 hepatocytes, with IC_{50} values greater than 100 μM. Conversely, the positive drug Harmine displayed obvious toxicity to both cell types at high concentrations, with the IC_{50} values of 39.57 μM and 28.95 μM, respectively.

2.5. Immunoblotting results

Previous studies have shown that the pathogenesis of AD is characterized by Tau overexpression and Aβ protein plaque deposition [33]. Meanwhile, the interaction between DYRK1A and Glycogen synthase kinase 3β (GSK-3β) synergistically induces the phosphorylation of Tau protein [34]. Accordingly, we assessed the expression of these proteins in SH-SY5Y cells. The representative bands obtained from the western blot assay are presented in Fig. 7a. As expected, the expression level of DYRK1A protein was higher in the OA-induced SH-SY5Y cell model than in the normal SH-SY5Y cells. Consistently, the levels of GSK-3β protein, GSK-3β (pSer9) protein, $A\beta_{1-42}$ protein, and Tau (pSer396)/Tau also increased in the OA-induced SH-SY5Y cell model. Interestingly, compound **L9** at both 1 μM and 10 μM reduced the levels of DYRK1A protein, GSK-3β protein, GSK-3β (pSer9) protein, $A\beta_{1-42}$ protein, and Tau (pSer396)/Tau, which was initially elevated in the OA-induced SH-SY5Y cell model (cf. Figure 7b-f). The immunoblotting assay revealed that compound **L9** effectively decreased the expression of AD-related proteins. These findings suggest that compound **L9** possessed potential anti-AD properties and we will perform *in vivo* study for further validation.

3. Conclusion

The DYRKA overexpression may cause the diseases such as AD, Parkinson's disease (PD), cancers, and diabetes. Therefore, DYRK1A inhibition is considered as a potential strategy to treat the aforementioned diseases. To date, many DYRK1A inhibitors have been identified, but none of them is approved for clinical use. Since the fate of several DYRK1A inhibitors in clinical trials or preclinical development is unpredictable, new chemotypes are still needed to circumvent the deficit of the know chemotypes, e.g. the toxicity of Harmine.

In this study, we employed pharmacophore filtering and molecular docking to screen our in-house chemical library. From that, we selected 10 diverse compounds for DYRK1A inhibition assay, and discovered compound **L9** as a moderately active DYRK1A inhibitor. The MD simulation has revealed the hydrogen bonds between compound **L9** and Glu239 and Leu241. According to the binding mode, the structural modification that could introduce hydrogen bond with Lys188 is likely to improve the potency of compound **L9**. Next, we used OA-induced SH-SY5Y cells as a model to test neuroprotective activity of compound **L9**. As expected, compound **L9** significantly ameliorated OA-induced cell injury in SH-SY5Y cells, by inhibiting the expression of DYRK1A as well as the related proteins GSK-3β and GSK-3β (pSer9) thereby reducing Tau protein hyperphosphorylation and Aβ deposition. By CCK-8 assay, we also observed that compound **L9** is not toxic to SH-SY5Y cells or HL-7702 hepatocytes.

Overall, we have discovered a novel DYRK1A inhibitor **L9** by using virtual screening and *in vitro* biological evaluation. Compound **L9** has also been experimentally validated at the cell level as a novel class of DYRK1A inhibitors with promising neuroprotective activity and thus worthy of further development.

4. Materials and Methods

4.1. Pharmacophore modeling

The pharmacophore models based on common features shared by active compounds were developed and validated using the HipHop module in Discovery Studio 2016 (v16.1.0, Dassault Systèmes Biovia Corp). In this study, a training set composed of six active compounds (Fig. 2a, A1-A6) from the article of Weber *et al.* [29] was built. Initially, the “Prepare Ligand” module was employed to add hydrogen atoms to each chemical structure and generate the protonation state at the pH of 7.4. Subsequently, the Principal and MaxOmitFeat properties of the chemical compounds were respectively defined. To be specific, the Principal and MaxOmitFeat properties were 2 and 0 for compounds **A1** and **A2**, respectively, and 1 for all the remaining compounds.

The “Genarate Conformations” module was utilized to generate up to 225 conformations per molecule at an energy interval of 20 kcal/mol. Next, the “Feature Mapping” module was employed to identify all pharmacophore features in the conformations. Among the 99 features, the most frequent ones were hydrogen bond acceptor (HBA), hydrogen bond donor (HBD), hydrophobic center (HYD), and aromatic ring (RA). Lastly, with the “Common Feature Pharmacophore Generation” module, the abovementioned features were selected. The allowed number of features in the pharmacophore was set to 0–5. The maximum number of models was 10. To evaluate the performance of the pharmacophore models, a test set composed of both highly active and weakly active compounds (Fig. 3a, A7-A22) from the same article of Weber *et al.* was built. The “Ligand Profiler” module was used to map the compounds in the test set to each pharmacophore model and generate a heatmap. Based on the heatmap, the pharmacophore models that exhibited the best performance were identified.

4.2. Virtual screening

4.2.1. Pharmacophore Filtering

The in-house compound library comprising 16,828 compounds was prepared by using the “Prepare Ligands” module. In the ligand preparation, the protonation state at pH of 7.4 and all the possible stereoisomers were generated. Subsequently, a multi-conformation database was constructed using the “Build 3D Database” module. In the database, each molecule had up to 255 conformations. The “Search 3D Database” module was used to map the molecules in the database to the optimal pharmacophore model based on the Fast algorithm. The fitness of each molecule to the pharmacophore model was assessed by the FitValue value, and all the molecules with FitValues greater than 1.5 were retained.

4.2.2. Molecular Docking

The crystal structure of human DYRK1A protein (PDB code: 6S14) was downloaded from PDB (https://www.rcsb.org/). The DYRK1A protein was prepared by the “Clean Protein” module of DS. The “Prepare Ligands” module was utilized to generate protonation states at the pH of 7.4 of the molecules.

Molecular docking was carried out using Smina [30], with the center of the coordinates of the active ligand and a radius of 8 Å defined as the active site. Protein-ligand docking was performed using the

Lamarckian Genetic Algorithm (LGA). The pose with the highest score was put out for each molecule. The scoring function was “Minimized Affinity” score. Consequently, ligands that formed hydrogen bonds with Lys188 or Leu241 were retained.

Molecular clustering was conducted the “Cluster Ligands” module of DS, with FCFP_6 as the fingerprints. In compound selection, the focus was on chemical structures with higher FitValues and lower Minimized Affinity scores, as well as better synthetic feasibility.

4.3. Molecular dynamics (MD) simulation

The molecule was redocked against the DYRK1A protein using smina, and the well-positioned pose was chosen to define the initial coordinates. Molecular dynamics simulation of the DYRK1A-ligand complex was conducted using GROMACS (version 2019.4) [31, 35]. Protein topology files were generated using the GROMOS96 43A1 force field, while ligand topology files were generated by the LigParGen server (http://zarbi.chem.yale.edu/ligpargen/) [36]. Molecular structures were optimized based on the Gaussian 09W software of the HF/6-31G* theory, and the charge distribution of the molecules was optimized using the RESP module in the AMBER21 software package. The simulations included energy minimization using steepest descent algorithm, 500-ps simulations at the equilibrium stage under NVT and NPT conditions, in which the system was maintained at a pressure of 1 atm using the Parrinello-Rahman method and at a constant temperature of 300 K using the V-rescale algorithm, and lastly the production simulation under NPT conditions for 100 ns.

4.4. Enzyme inhibition assay

The protocol of this assay was similar to the published one [37]. The activity against DYRK1A was assessed in 384-well plates using the ADP-Glo Kinase Assay kit (Promega), with Harmine as the positive control. The kinase reaction involving DYRK1A was conducted in a kinase buffer comprising 50 mM Hepes (Thermo), 20 mM $MgCl_2$ (Sigma), 0.01% Brij35 (Millipore), 1 mM EGTA (Sigma), and 2 mM DTT (MCE). The ATP substrate solution and the DYRK1A kinase solution were prepared using the same buffer, and the test samples were dissolved in DMSO at the indicated concentrations. Next, the ADP-Glo Kinase Reagent was added to terminate the kinase reaction, and the mixture was further incubated at 25°C for 40 min. Lastly, the Kinase Detection Reagent was added and incubated for 40 min at 25°C. The activity (%) of DYRK1A at various concentrations was determined based on the luminescence, and the IC_{50} value was calculated using GraphPad Prism software (GraphPad Software Inc., La Jolla, CA).

4.5. Cell Culture

SH-SY5Y cells were obtained from Jiangsu Kaiji Biotechnology Co. The cells were cultured with high glucose DMEM medium (KeyGEN, China) containing 10% fetal bovine serum (Hangzhou Sijiqing, China), 1% penicillin and streptomycin, in an incubator at 37 ℃ and with 5% CO_2. All the cells were sub-cultured for 3 to 5 generations for experiments.

4.6. CCK-8 assay

In the neuroprotection assays, SH-SY5Y cells were seeded in 96-well plates at a density of 5×10^3 cells per well for 24 h. The cells were then treated with or without compounds (dissolved in DMSO) at the indicated concentrations. 100 nM OA (yuanye Bio-Technology, China) was added to each well after 24 h. Cell viability was analyzed by CCK-8 (Solarbio, China) after 24 h. To be specific, 10 μL of CCK-8 solution was added to the cells, and incubated at 37°C for 2 h. The optical density (OD) was measured using a Microplate Reader (TECAN, Switzerland) at 450 nm, and cell viability was expressed as percentage% (compared to negative control). Each assay was repeated at least three times. Harmine was used as the reference compound [38].

In the cytotoxicity assays, SH-SY5Y cells and HL-7702 cells were respectively cultured in 96-well plates until 40–50% confluence was reached. The compound was added at final concentrations of 100 nM, 333 nM, 1 μM, 3 μM, 10 μM, 33 μM, and 100 μM. After 24 h, cell viability was assessed at a wavelength of 450 nm, based on the same protocol mentioned above.

4.7. Western blot assay

The cells were collected in RIPA lysate (Solarbio, China) supplemented with 1% benzyl sulfonyl fluoride (Solarbio, China) and 1% protein phosphatase inhibitor (Solarbio, China), and then placed on ice for 30 min and subsequently centrifuged at 4°C and 12,000 rpm for 15 min. The protein concentration was determined using the BCA assay (Beyotime, China). Equal amounts of protein samples were separated and transferred to the 8–12% SDS-PAGE and PVDF membranes. After a 2h blocking step at room temperature using 5% non-fat dry milk in TBS-Tween-20 (0.1%, v/v), the membranes were incubated overnight at 4°C with primary antibodies, including anti-DYRK1A (1:1000, Abcam, UK), anti-GSK-3β (1:1000, Abcam, UK), anti-GSK-3β (pSer9) (1:1000, Abcam, UK), anti-Tau (pSer396) (1:1000, Abcam, UK), anti-Tau (1:500, Thermo Fisher Scientific, USA), anti-$A\beta_{1-42}$ (1:1000, Proteintech, China) or anti-β-actin antibody (1:1000, Zsbio, China). β-actin was used as the internal control. Subsequently, the membranes were incubated with a secondary antibody (1:3000, Abcam, UK) for 1 h at room temperature. The Amersham Imager 600 (GE, USA) was used to measure the blots. Image-J software was used to examine the strip's grayscale data after film scanning.

Declarations

ASSOCIATED CONTENT

Declaration of competing interest

The authors declare that they have no known competing financial interests or personal relationships that could have appeared to influence the work reported in this paper.

Author Contributions

Conception of the hypothesis: Jie Xia; Study supervision: Jie Xia, Xuehui Zhang, Hao Wang; Data acquisition, analysis and interpretation: Xinxin Si, Chenliang Qian, Yaling Wang, Mingli Yao (for

computational modeling) and Nianzhuang Qiu (for biology); Writing, review, and/or revision of the manuscript: XinXin Si, Chenliang Qian, Nianzhuang Qiu, Jie Xia and Xuehui Zhang. The manuscript is written through contributions of all authors. All authors have given approval to the final version of the manuscript.

Acknowledgments

This work is partly supported by the CAMS Innovation Fund for Medical Sciences (Grant No. 2021-I2M-1-069). We thank Dr. Igor V. Tetko (Institute of Structural Biology, Helmholtz Zentrum München-Research Center for Environmental Health) for the constructive suggestions and the support by the Program for Foreign Talent of Ministry of Science and Technology of the People's Republic of China (Grant No. G2021194015L).

References

1. Park J, Song WJ, Chung KC: **Function and regulation of Dyrk1A: towards understanding Down syndrome.** *Cell Mol Life Sci* 2009, **66:**3235-3240.
2. Park J, Oh Y, Chung KC: **Two key genes closely implicated with the neuropathological characteristics in Down syndrome: DYRK1A and RCAN1.** *BMB Rep* 2009, **42:**6-15.
3. Alvarez M, Estivill X, de la Luna S: **DYRK1A accumulates in splicing speckles through a novel targeting signal and induces speckle disassembly.** *J Cell Sci* 2003, **116:**3099-3107.
4. Aranda S, Laguna A, de la Luna S: **DYRK family of protein kinases: evolutionary relationships, biochemical properties, and functional roles.** *Faseb j* 2011, **25:**449-462.
5. Himpel S, Tegge W, Frank R, Leder S, Joost HG, Becker W: **Specificity determinants of substrate recognition by the protein kinase DYRK1A.** *J Biol Chem* 2000, **275:**2431-2438.
6. Demuro S, Di Martino RMC, Ortega JA, Cavalli A: **GSK-3β, FYN, and DYRK1A: Master Regulators in Neurodegenerative Pathways.** *Int J Mol Sci* 2021, **22**.
7. Khor B, Gagnon JD, Goel G, Roche MI, Conway KL, Tran K, Aldrich LN, Sundberg TB, Paterson AM, Mordecai S, et al: **The kinase DYRK1A reciprocally regulates the differentiation of Th17 and regulatory T cells.** *Elife* 2015, **4**.
8. Rozen EJ, Roewenstrunk J, Barallobre MJ, Di Vona C, Jung C, Figueiredo AF, Luna J, Fillat C, Arbonés ML, Graupera M, et al: **DYRK1A Kinase Positively Regulates Angiogenic Responses in Endothelial Cells.** *Cell Rep* 2018, **23:**1867-1878.
9. Feki A, Hibaoui Y: **DYRK1A Protein, A Promising Therapeutic Target to Improve Cognitive Deficits in Down Syndrome.** *Brain Sci* 2018, **8**.
10. Smith B, Medda F, Gokhale V, Dunckley T, Hulme C: **Recent advances in the design, synthesis, and biological evaluation of selective DYRK1A inhibitors: a new avenue for a disease modifying treatment of Alzheimer's?** *ACS Chem Neurosci* 2012, **3:**857-872.

11. Wegiel J, Gong CX, Hwang YW: **The role of DYRK1A in neurodegenerative diseases.** *Febs j* 2011, **278:**236-245.
12. Fernández-Martínez P, Zahonero C, Sánchez-Gómez P: **DYRK1A: the double-edged kinase as a protagonist in cell growth and tumorigenesis.** *Mol Cell Oncol* 2015, **2:**e970048.
13. Uhl KL, Schultz CR, Geerts D, Bachmann AS: **Harmine, a dual-specificity tyrosine phosphorylation-regulated kinase (DYRK) inhibitor induces caspase-mediated apoptosis in neuroblastoma.** *Cancer Cell Int* 2018, **18:**82.
14. Ackeifi C, Swartz E, Kumar K, Liu H, Chalada S, Karakose E, Scott DK, Garcia-Ocaña A, Sanchez R, DeVita RJ, et al: **Pharmacologic and genetic approaches define human pancreatic β cell mitogenic targets of DYRK1A inhibitors.** *JCI Insight* 2020, **5**.
15. Ackeifi C, Wang P, Karakose E, Manning Fox JE, González BJ, Liu H, Wilson J, Swartz E, Berrouet C, Li Y, et al: **GLP-1 receptor agonists synergize with DYRK1A inhibitors to potentiate functional human β cell regeneration.** *Sci Transl Med* 2020, **12**.
16. Belgardt BF, Lammert E: **DYRK1A: A Promising Drug Target for Islet Transplant-Based Diabetes Therapies.** *Diabetes* 2016, **65:**1496-1498.
17. Bain J, Plater L, Elliott M, Shpiro N, Hastie CJ, McLauchlan H, Klevernic I, Arthur JS, Alessi DR, Cohen P: **The selectivity of protein kinase inhibitors: a further update.** *Biochem J* 2007, **408:**297-315.
18. de la Torre R, de Sola S, Hernandez G, Farré M, Pujol J, Rodriguez J, Espadaler JM, Langohr K, Cuenca-Royo A, Principe A, et al: **Safety and efficacy of cognitive training plus epigallocatechin-3-gallate in young adults with Down's syndrome (TESDAD): a double-blind, randomised, placebo-controlled, phase 2 trial.** *Lancet Neurol* 2016, **15:**801-810.
19. Göckler N, Jofre G, Papadopoulos C, Soppa U, Tejedor FJ, Becker W: **Harmine specifically inhibits protein kinase DYRK1A and interferes with neurite formation.** *Febs j* 2009, **276:**6324-6337.
20. Debdab M, Carreaux F, Renault S, Soundararajan M, Fedorov O, Filippakopoulos P, Lozach O, Babault L, Tahtouh T, Baratte B, et al: **Leucettines, a class of potent inhibitors of cdc2-like kinases and dual specificity, tyrosine phosphorylation regulated kinases derived from the marine sponge leucettamine B: modulation of alternative pre-RNA splicing.** *J Med Chem* 2011, **54:**4172-4186.
21. Nguyen TL, Duchon A, Manousopoulou A, Loaëc N, Villiers B, Pani G, Karatas M, Mechling AE, Harsan LA, Limanton E, et al: **Correction of cognitive deficits in mouse models of Down syndrome by a pharmacological inhibitor of DYRK1A.** *Dis Model Mech* 2018, **11**.
22. Ogawa Y, Nonaka Y, Goto T, Ohnishi E, Hiramatsu T, Kii I, Yoshida M, Ikura T, Onogi H, Shibuya H, et al: **Development of a novel selective inhibitor of the Down syndrome-related kinase Dyrk1A.** *Nat Commun* 2010, **1:**86.
23. Deshmukh V, Hu H, Barroga C, Bossard C, Kc S, Dellamary L, Stewart J, Chiu K, Ibanez M, Pedraza M, et al: **A small-molecule inhibitor of the Wnt pathway (SM04690) as a potential disease modifying agent for the treatment of osteoarthritis of the knee.** *Osteoarthritis Cartilage* 2018, **26:**18-27.
24. Deshmukh V, O'Green AL, Bossard C, Seo T, Lamangan L, Ibanez M, Ghias A, Lai C, Do L, Cho S, et al: **Modulation of the Wnt pathway through inhibition of CLK2 and DYRK1A by lorecivivint as a novel,**

potentially disease-modifying approach for knee osteoarthritis treatment. *Osteoarthritis Cartilage* 2019, **27:**1347-1360.

25. Melchior B, Mittapalli GK, Lai C, Duong-Polk K, Stewart J, Güner B, Hofilena B, Tjitro A, Anderson SD, Herman DS, et al: **Tau pathology reduction with SM07883, a novel, potent, and selective oral DYRK1A inhibitor: A potential therapeutic for Alzheimer's disease.** *Aging Cell* 2019, **18:**e13000.
26. Gourdain S, Dairou J, Denhez C, Bui LC, Rodrigues-Lima F, Janel N, Delabar JM, Cariou K, Dodd RH: **Development of DANDYs, new 3,5-diaryl-7-azaindoles demonstrating potent DYRK1A kinase inhibitory activity.** *J Med Chem* 2013, **56:**9569-9585.
27. Metz JT, Johnson EF, Soni NB, Merta PJ, Kifle L, Hajduk PJ: **Navigating the kinome.** *Nat Chem Biol* 2011, **7:**200-202.
28. Koyama T, Yamaotsu N, Nakagome I, Ozawa SI, Yoshida T, Hayakawa D, Hirono S: **Multi-step virtual screening to develop selective DYRK1A inhibitors.** *J Mol Graph Model* 2017, **72:**229-239.
29. Weber C, Sipos M, Paczal A, Balint B, Kun V, Foloppe N, Dokurno P, Massey AJ, Walmsley DL, Hubbard RE, et al: **Structure-Guided Discovery of Potent and Selective DYRK1A Inhibitors.** *J Med Chem* 2021, **64:**6745-6764.
30. Koes DR, Baumgartner MP, Camacho CJ: **Lessons learned in empirical scoring with smina from the CSAR 2011 benchmarking exercise.** *J Chem Inf Model* 2013, **53:**1893-1904.
31. Scott WRP, Hünenberger PH, Tironi IG, Mark AE, Billeter SR, Fennen J, Torda AE, Huber T, Krüger P, van Gunsteren WF: **The GROMOS Biomolecular Simulation Program Package.** *The Journal of Physical Chemistry A* 1999, **103:**3596-3607.
32. Henderson SH, Sorrell F, Bennett J, Fedorov O, Hanley MT, Godoi PH, Ruela de Sousa R, Robinson S, Ashall-Kelly A, Hopkins Navratilova I, et al: **Discovery and Characterization of Selective and Ligand-Efficient DYRK Inhibitors.** *J Med Chem* 2021, **64:**11709-11728.
33. Ryoo SR, Cho HJ, Lee HW, Jeong HK, Radnaabazar C, Kim YS, Kim MJ, Son MY, Seo H, Chung SH, Song WJ: **Dual-specificity tyrosine(Y)-phosphorylation regulated kinase 1A-mediated phosphorylation of amyloid precursor protein: evidence for a functional link between Down syndrome and Alzheimer's disease.** *J Neurochem* 2008, **104:**1333-1344.
34. Woods YL, Cohen P, Becker W, Jakes R, Goedert M, Wang X, Proud CG: **The kinase DYRK phosphorylates protein-synthesis initiation factor eIF2Bepsilon at Ser539 and the microtubule-associated protein tau at Thr212: potential role for DYRK as a glycogen synthase kinase 3-priming kinase.** *Biochem J* 2001, **355:**609-615.
35. Christen M, Hünenberger PH, Bakowies D, Baron R, Bürgi R, Geerke DP, Heinz TN, Kastenholz MA, Kräutler V, Oostenbrink C, et al: **The GROMOS software for biomolecular simulation: GROMOS05.** *J Comput Chem* 2005, **26:**1719-1751.
36. Dodda LS, Cabeza de Vaca I, Tirado-Rives J, Jorgensen WL: **LigParGen web server: an automatic OPLS-AA parameter generator for organic ligands.** *Nucleic Acids Res* 2017, **45:**W331-w336.
37. Lechner C, Flaßhoff M, Falke H, Preu L, Loaëc N, Meijer L, Knapp S, Chaikuad A, Kunick C: **[b]-Annulated Halogen-Substituted Indoles as Potential DYRK1A Inhibitors.** *Molecules* 2019, **24**.

38. Berdigaliyev N, Aljofan M: **An overview of drug discovery and development.** *Future Med Chem* 2020, **12:**939-947.

Table

Table 2 is available in the Supplementary Files section.

Scheme

Scheme 1 is available in the Supplementary Files section.

Figures

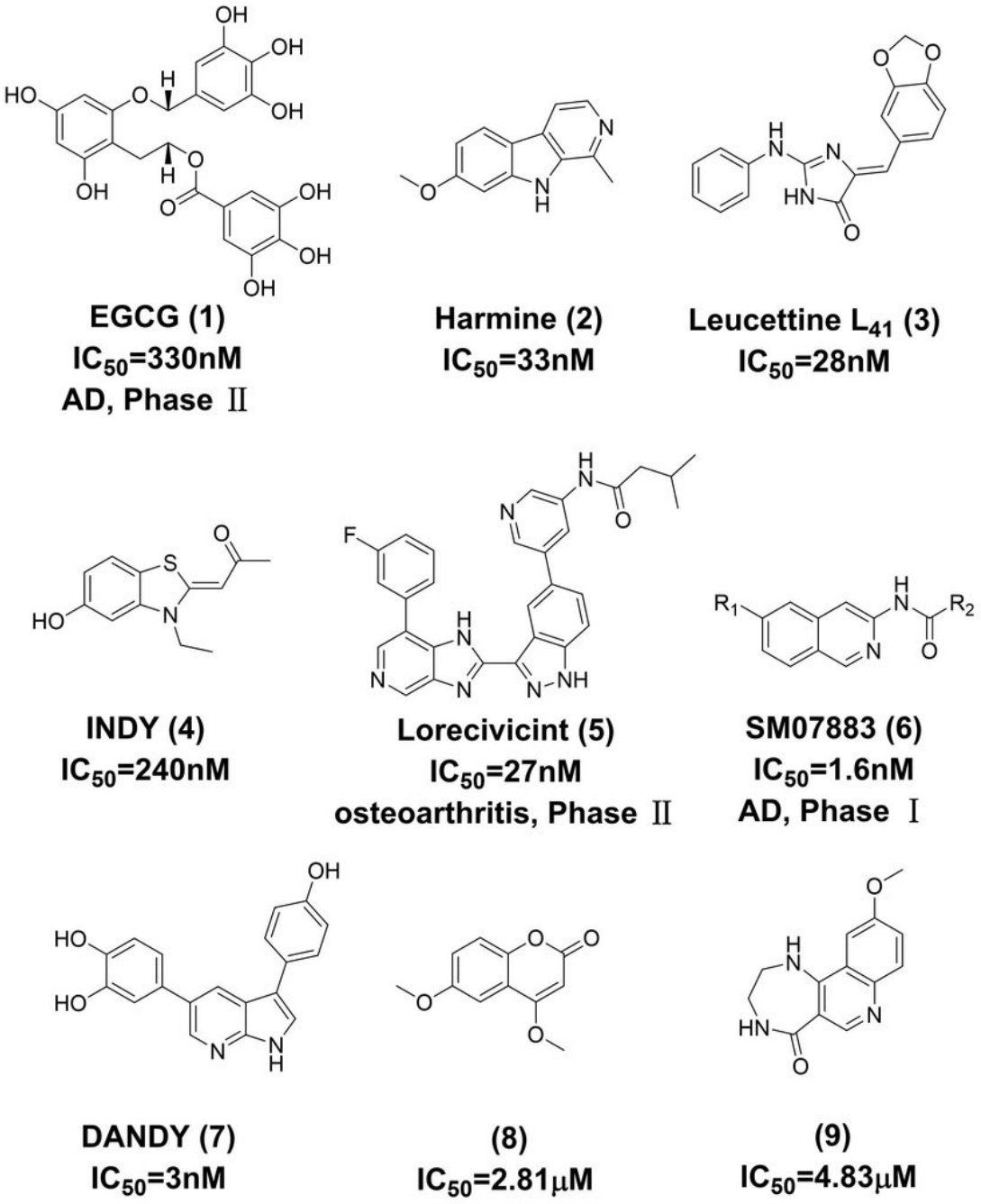

Figure 1

Chemical structures of known DYRK1A inhibitors.

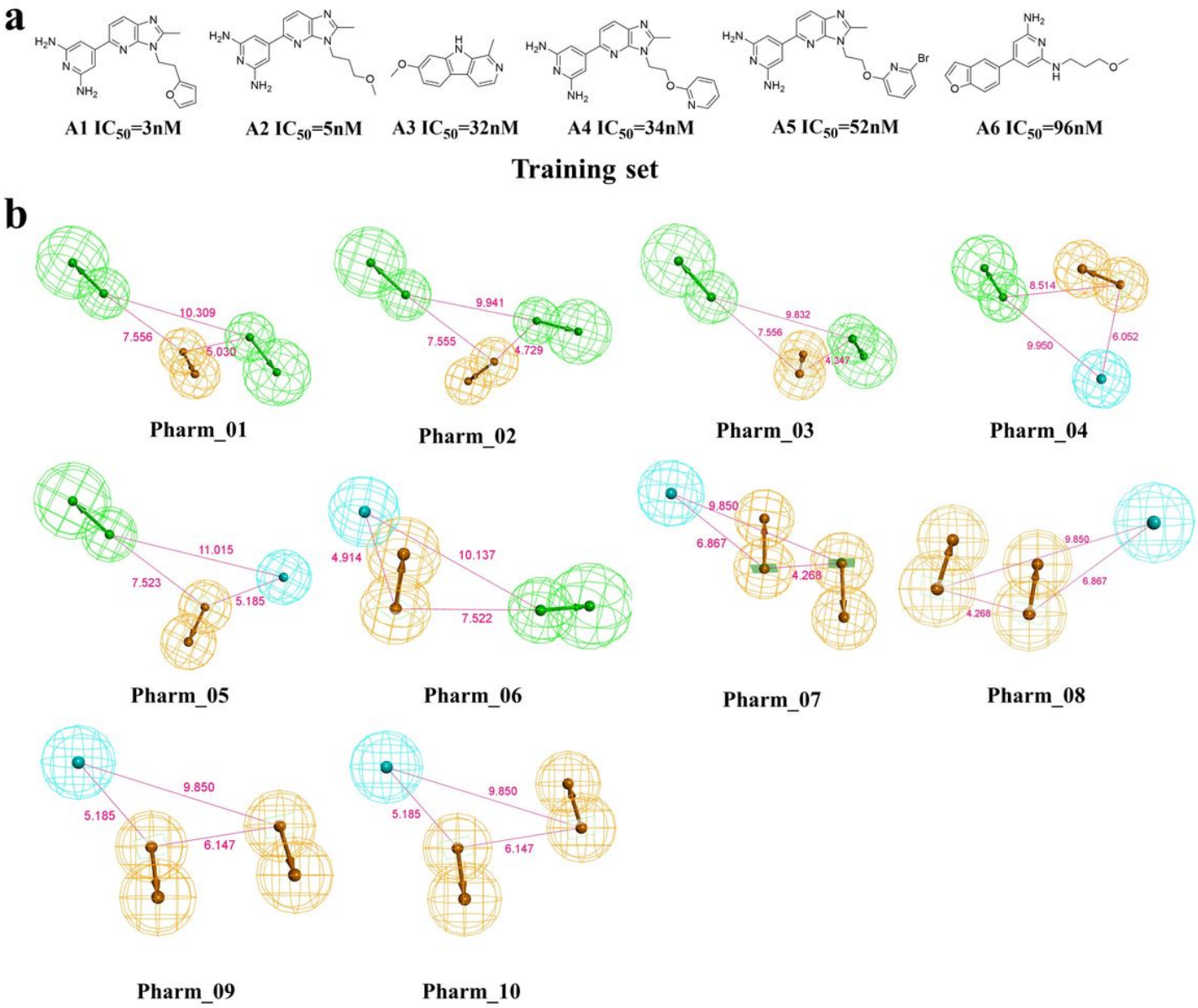

Figure 2

The building of common-feature pharmacophores. (a) Training set for building pharmacophore models. (b) 10 pharmacophore models constructed by Discovery Studio. The features are colored: ring aromatic (orange), general hydrophobic feature (blue) and hydrogen bond acceptor (green).

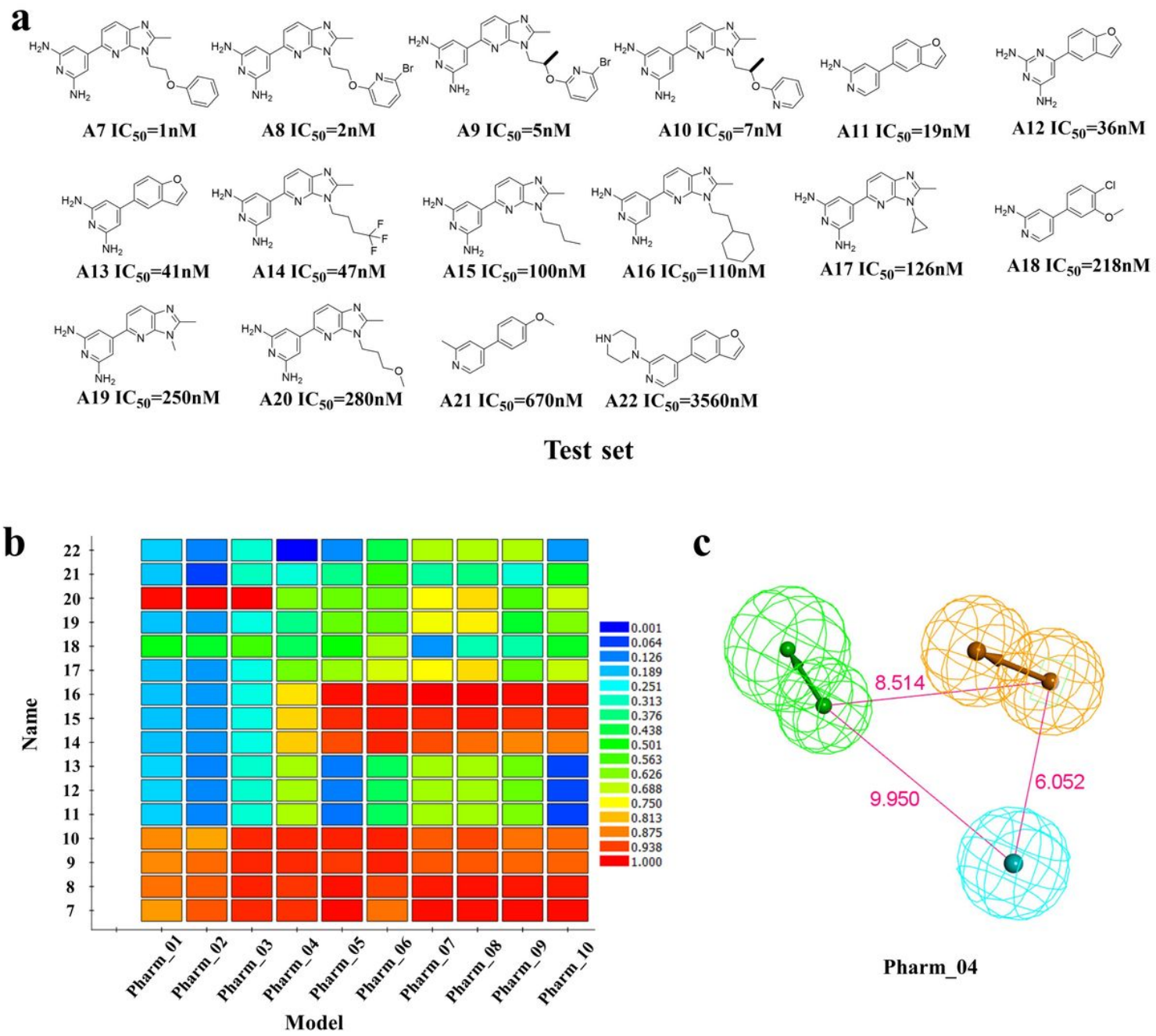

Figure 3

Model validation and selection of the optimal model. (a) Chemical structures of the DYRK1A inhibitors in the test set; (b) The molecules in the test set are mapped to each pharmacophore model; (c) The optimal common-feature pharmacophore model. The model is composed of one ring aromatic (orange), one general hydrophobic feature (blue) and one hydrogen bond acceptor (green). The distances between two features are also shown (unit: Å).

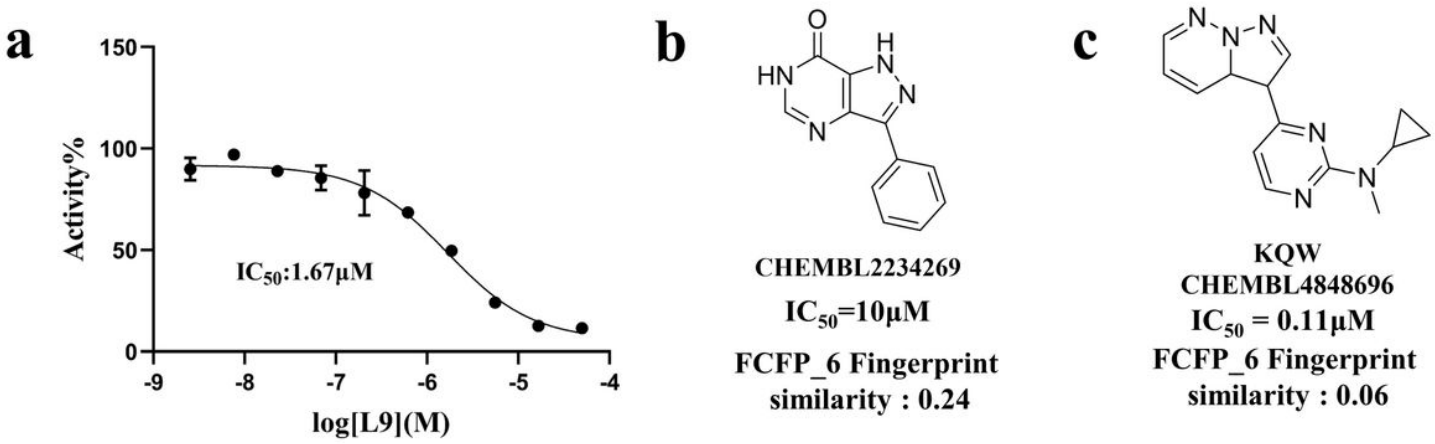

Figure 4

The activity and structural novelty of compound **L9**. (a) Dose-response curve of compound **L9** for DYRK1A inhibition; (b) The DYRK1A inhibitor from ChEMBL33 that was the most similar to compound **L9**; (c) The structural similarity (Tanimoto coefficient) based on FCFP_6 fingerprints between compound **L9** and the cognate ligand **KQW** from the cocrystal structure used for molecular docking.

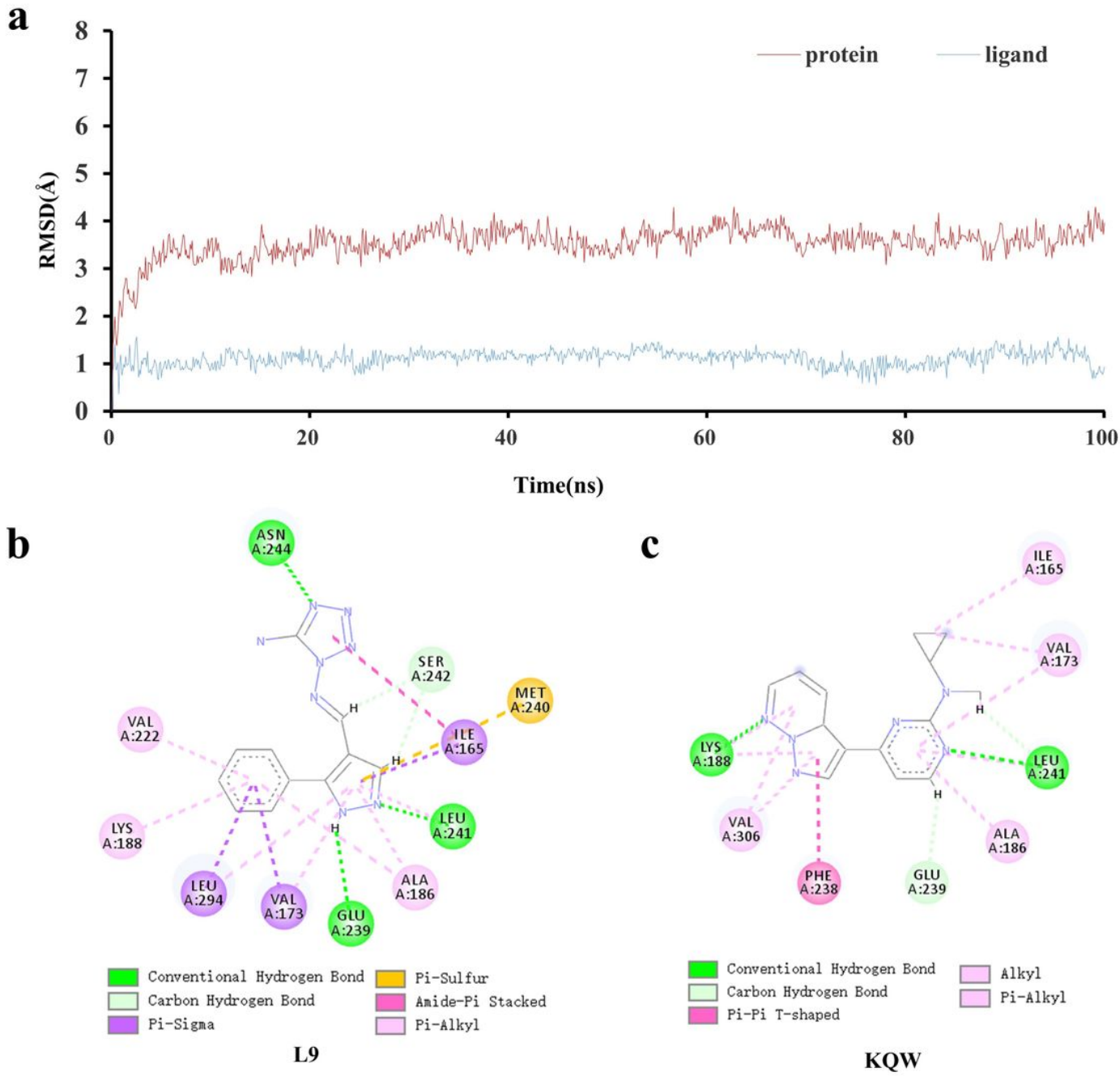

Figure 5

The binding details of compound **L9** to DYRK1A. (a) The Heavy-atom RMSDs of DYRK1A and the ligand as a function of time during the 100-ns MD simulations. The RMSD was calculated with the starting conformation/pose as the reference. (b) Binding mode of compound **L9** to DYRK1A. (c) Binding mode of ligand **KQW** to DYRK1A (PDB code: 6S14). Images were created with Discovery Studio 2016.

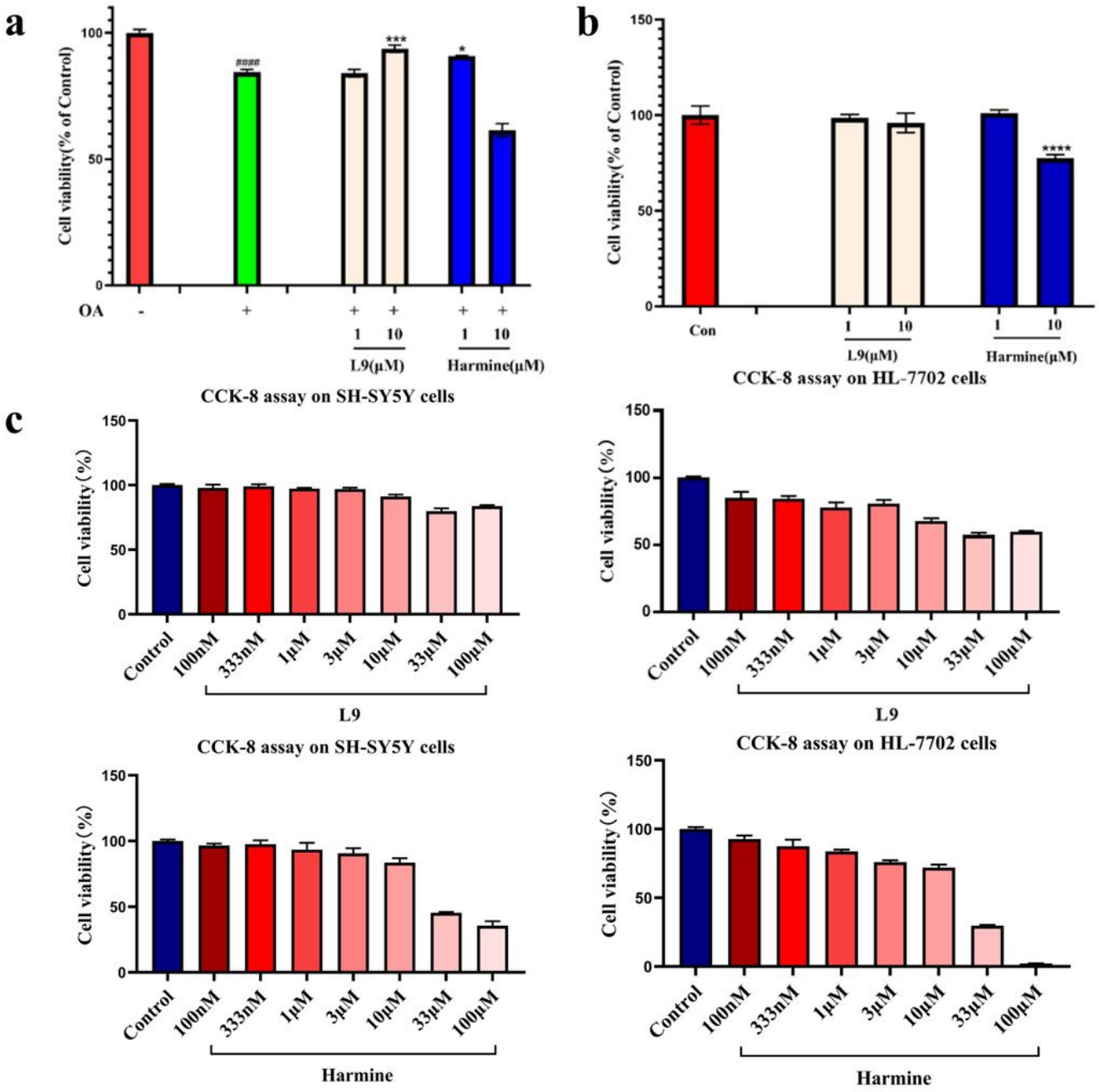

Figure 6

The neuroprotective activity of compound **L9**. (a) Effect of compound **L9** on OA-induced SH-SY5Y cell viability. (b) Effect of the compounds on the viability of SH-SY5Y cells. The results are presented as mean ± SEM (n = 3). $^{\#\#\#\#}p < 0.0001$ vs the control group. $^{*}p < 0.05$, $^{***}p < 0.001$, $^{****}p < 0.0001$ vs the OA (100 nM) group. (c) The toxicity of compound **L9** to SH-SY5Y cells and HL-7702 hepatocytes (Harmine as the reference compound).

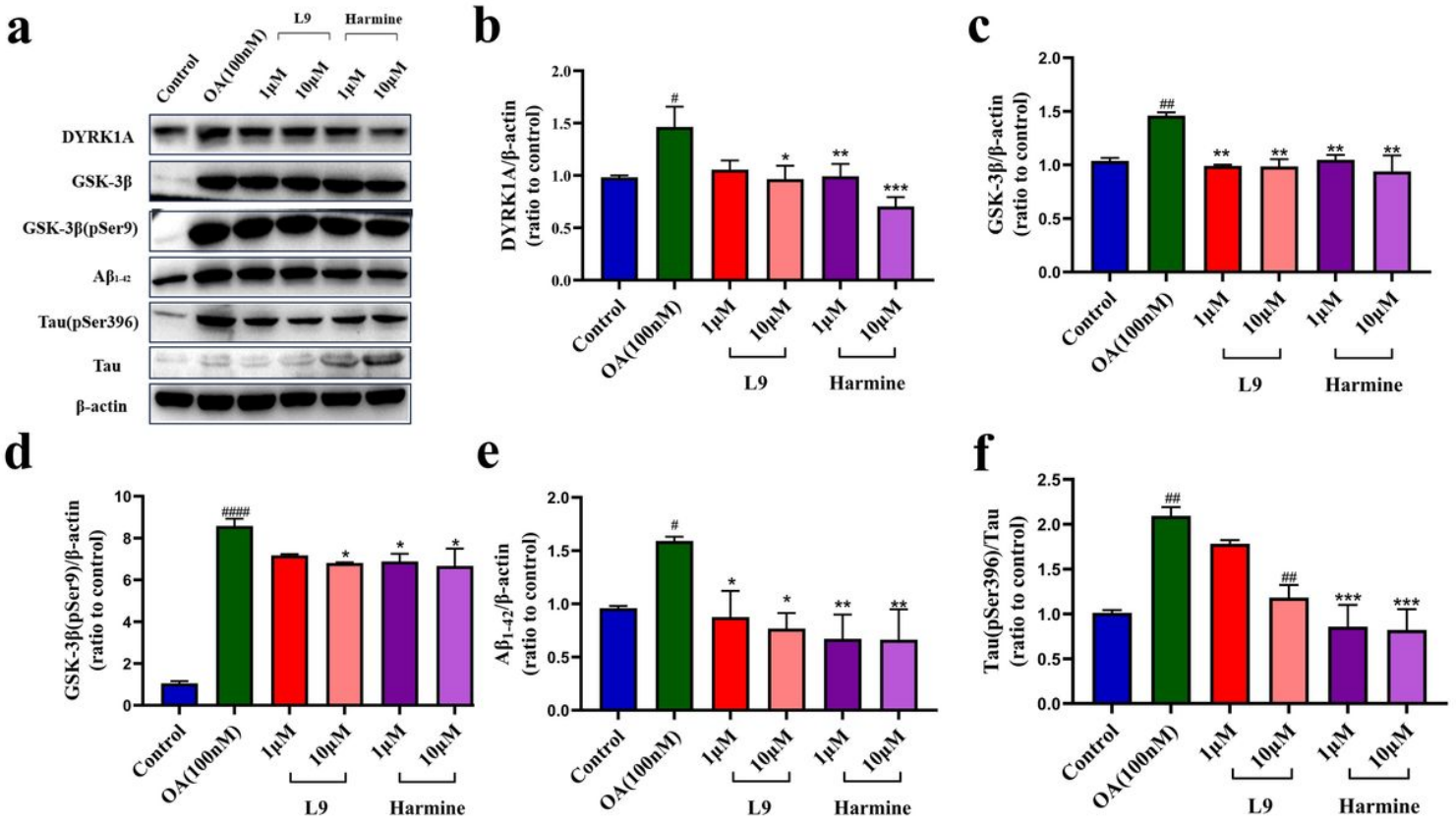

Figure 7

The mechanism of compound **L9** for neuroprotection. (a) The effect of compound **L9** on OA-induced protein expression in SH-SY5Y cells. Representative images are shown. (b-f) Quantification of DYRK1A expression (b), GSK-3β expression (c), GSK-3β (pSer9) expression (d), $A\beta_{1-42}$ expression (e) and Tau (Ser396)/Tau(f). The results are presented as mean ± SEM (n = 3). $^{\#}p < 0.05$, $^{\#\#}p < 0.01$, $^{\#\#\#\#}p<0.0001$ vs the control group. $^{*}p < 0.05$, $^{**}p < 0.01$, $^{***}p < 0.001$, vs the OA (100 nM) group. Harmine was used as a positive drug.

Supplementary Files

This is a list of supplementary files associated with this preprint. Click to download.

- Table2.docx
- GraphicalAbstract.jpg
- Scheme1.jpg